Low-Density Wireless Sensor Networks for Localization and Tracking in Critical Environments

Angelo Cenedese, Giulia Ortolan, and Marco Bertinato

***Abstract*—In this paper, the problem of localizing and tracking mobile nodes acting in a fixed wireless sensor network (WSN) is addressed. A strategy is proposed based on an empirical map of the received signal-strength distribution that is generated by the WSN and on a stochastic model of the mobile-node behavior. This approach results in being well suited for low-density setups and critical environments. The theoretical background and the architecture of the system are presented, together with simulations to validate the design phase. Also, the system is implemented into a real-time framework, and its performance is tested in an industrial indoor environment.**

***Index Terms*—Estimation theory, localization and tracking, packet loss, random walk model, stochastic modeling, wireless sensor networks.**

I. Introduction

WIRELESS sensor networks (WSNs), which are large networks of spatially distributed electronic devices (nodes) capable of sensing, computation, and wireless communication, are becoming very popular not only within the academic community as a prototype for multiagent systems but in industry as well. In fact, they can offer access to unprecedented quality and quantity of information that can revolutionize our ability to control the environment: Typical applications include building environmental control [1], vehicular networks [2], surveillance [3], habitat monitoring [4], [5], and manufacturing automation [6]. In particular, location-based applications are among the first and most popular applications of WSNs since they can be employed to track people in wide outdoor areas or enemies in the battlefield or in extending to indoor environments the GPS approach for locating people and tracking mobile objects in large buildings (e.g., warehouses, hospitals). The work in this paper is motivated by one of these applications, i.e., the design of a real-time system that can support fire-rescue squads to locate them and to navigate through a building during emergency scenarios. Moreover, to improve coordinated searching strategies, there might also be a need to communicate a fireman's position to an external unit supervising operations.

To achieve these objectives, we propose deploying a static WSN whose nodes are placed in known positions. Each mobile subject is then provided with a compact smart device [personal digital assistant (PDA)-like] that can communicate with the static network and compute and transmit the estimated current position. In detail, the position of the node is obtained using only the radio signals [received signal strength (RSS)] that are provided by a standard IEEE 802.15.4 radio chip, without resorting to any other special sensors or devices such as infrared (IR) motion sensors, ultrasound, or directional antennas.

The entire network of both fixed and mobile nodes (MNs) then realizes a distributed intelligence system, relying on the computational capabilities of the nodes. In this framework, however, local position computation is performed by the mobile unit, allowing inherent robustness to static node failure and scalability of the system since the static network simply keeps on transmitting its own location, regardless of the number of MNs in the area. Each PDA computes its own position and displays it on a screen with a map of the environment similarly to commercial GPS-based navigation systems. The position is also transmitted to the static network, which routes it back to a gateway and, finally, to the outer coordination center.

In addition, the localization system must also comply with a number of constraints that are common to WSNs. In fact, it needs to be power-efficient if the nodes of the static network are battery-powered, to be robust to packet drop, and to run in real time, and finally, it should maintain acceptable localization accuracy, even in the event of some static node failure.

To avoid confusion, some definitions are in order before proceeding: We define *localization* as the process of estimating the position of a node, whereas *tracking* is the process of estimating the trajectory of a moving node, possibly adopting a model of the object dynamics to reduce localization error.

In recent years, the problems of localization and tracking have been widely explored with particular emphasis on the accuracy issue: On the other hand, however, the localization error is not the only important factor that needs to be considered when designing an appropriate system. Other aspects are important such as the number of nodes to achieve a desired localization error, the computational requirements that are necessary to run the proposed algorithms in real time, the installation and maintenance costs, the system lifetime, the robustness to packet drop and node failures, and the system scalability.

In this spirit, the contribution of this paper is twofold. On the theoretical side, the proposed approach belongs to RSS map-based localization systems and makes use of a stochastic model

Manuscript received September 21, 2009; revised February 19, 2010; accepted April 11, 2010. Date of publication April 29, 2010; date of current version July 16, 2010. This work was supported in part by the European Community's The Seventh Framework Programme (FP7) under Agreement FP7-ICT-223866-FeedNetBack and in part by the Italian CaRiPaRo Foundation Project "Wise-Wai." The review of this paper was coordinated by Prof. H. Hassanein.

A. Cenedese is with the Department of Engineering and Management, University of Padova, 36100 Vicenza, Italy (e-mail: angelo.cenedese@unipd.it).

G. Ortolan is with the Department of Information Engineering, University of Padova, 35131 Padova, Italy.

M. Bertinato was with the Department of Engineering and Management, University of Padova, 36100 Vicenza, Italy. He is now with Aprilia Racing S.r.l., Piaggio & Co. Group, R&D Department, Noale, Italy.

Digital Object Identifier 10.1109/TVT.2010.2049277

relying on empirical RSS measurements that are collected in the real environment, similarly to that proposed in [7], but adopting, in addition, a novel interpolation for the RSS map. Also, packet-loss channel modeling has been studied and integrated into the system. On a more practical ground, the system has been evaluated both in simulation and real-world experiments, with particular attention to issues such as the extension of the static network coverage without excessive increase in the number of nodes and the communication loss in the network. The architecture is implemented in a real-world testbed using commercial-off-the-shelf wireless sensor nodes, hardware, and software, and the static network deployment procedure undergoes a connectivity analysis step and a heuristic optimal placement of sensors. Finally, real-time tracking experiments are performed in a rather hostile and large-scale indoor environment that is characterized by massive concrete walls, high electromagnetic interference, and metallic structures.

Interestingly, a similar application project, in principle, has been developed by the University of Berkeley and is called the *Fire Information and Rescue Equipment (FIRE)* [8]. The FIRE system is designed for working firemen and is composed of two basic elements: 1) *SmokeNet*, which is a static WSN and is able to monitor environmental parameters and to locate each fireman inside the area of interest; and 2) *FireEye*, which is a custom-made fireman equipment that includes a helmet with a navigation liquid-crystal-display monitor.

The remainder of this paper is organized as follows. After a brief review of the state of the art (see Section II), in Section III, the problem is presented in a formal approach, and the steps for the design of a localization system are described in detail. Then, in Sections IV and V, simulations and real-world experiments to assess and validate the proposed architecture and algorithms are presented, respectively. Finally, in Section VII, some considerations on the results are drawn.

II. State of the Art

Within the context of WSNs, localization algorithms can be classified according to the parameter that is used to get relative position information between nodes as, among others, the *angle of arrival* (AoA; an estimate of the relative angles between nodes), the *time of arrival* (the time that is taken by the radio signal to propagate from one node to another), the *time difference of arrival* (TDoA; the time interval between the reception of a radio signal and an ultrasound that is emitted by a beacon), and the *RSS* (an index of the received signal power). Approaches based on the first three quantities require specific devices such as array antennas for the AoA [9], ultrasound modules for TDoA [10], dedicated hardware and software to maintain node synchronization [11], or motion detection sensors such as magnetometers and IR motion sensors [3]. Although successful implementations of systems based on these approaches exist, they are not widespread because the specific localization hardware is too expensive or fragile in cluttered and dynamic environments.

Differently, RSS localization systems are much more popular since most of today's radio chips for WSNs provide them at no extra hardware cost. In an ideal medium with an ideal antenna, there should be an information-preserving correspondence between each RSS value and the relative distance between two nodes; however, in an indoor environment, multipath fading, reflections, diffraction, interference, and the presence of dynamics highly affect this relation. Although the localization accuracy is poorer than the one achieved with the non-RSS localization systems, it is sufficient in many applications, such as the one addressed in this paper. Moreover, most of the algorithms coping with the high variability of RSS measurements can be grouped into two distinct classes, which are referred to as *RSS-map-matching*-based localization and *RSS-channel-model*-based localization, given a common architecture composed of a set of static nodes that are placed at fixed locations in the environment and a set of MNs to be localized.

The first class of algorithms is based on the RSS maps that are generated by each static wireless node. In particular, these maps take into account the location of the static nodes, as well as the topology and the morphology of the environment, including walls and static objects. The most popular tracking systems in this class are RADAR [12] and MoteTrack [13]. The RSS map is obtained either by exploiting an analytical model of propagation of the radio signal [14] or by dedicated measurement campaigns. The *analytical* RSS map can be provided by standard tools like ray tracing [15]; however, it does not take into account small objects like tables and shelves or dynamics in the environment, thus possibly leading to poor performance. The *empirical* RSS map, instead, better represents the real situation but requires an extensive set of experiments [7]. From a different point of view, the RSS map can be *deterministic* or *stochastic*, with the former associating to each point (x, y, z) of the environment a single RSS value for each node, and the latter resorting to a probability distribution of RSS values: The stochastic RSS map is more realistic than the deterministic one, as it takes into account possible dynamic variations of the environment at the price, however, of a more complex model [7], [16]. In all these cases, the maps are computed offline for each static node, giving for any point in the environment the corresponding RSS value or its probabilistic distribution: Position estimates of MNs are then calculated online by searching for a value that is closest to the current measurement in terms of some defined metric, provided that searching for the best match in the RSS map can be computationally expensive if the map is finely gridded. To overcome this problem, for example, RADAR adopts a technique called the *nearest neighbor in signal space* to identify a subset of possible positions aiming at reducing the computation time that is required for the location estimate. MoteTrack adopts a similar strategy, called the reference signature, which also implements features that reduce estimation errors, improving robustness and scalability at the same time. Both RADAR and MoteTrack are based on a deterministic model for the RSS map. If the RSS maps are generated with a probabilistic method, the location of the tracked node can be obtained by computing the most likely location based on the received measurements using a Bayesian approach. Recently, the multiple-transmit power information has also been taken into account to model RSS maps [17]. This strategy is more computationally expensive but also yields good performance in highly cluttered indoor environments.

Differently, the algorithms based on an RSS channel model first try to estimate the relative distance between the moving node and the static nodes and then use a geometric approach to triangulate the location of the former. The advantage of this strategy relies on the fact that no *a priori* detailed RSS map of the environment is required, and the localization algorithms are computationally efficient. In particular, the distance-versus-RSS model is based on a fading-channel model with Gaussian noise, and the distance is derived using a maximum-likelihood estimator [18]. Once the relative distances from each anchor node (AN) are obtained, the triangulation technique calculates the location of the moving target by solving a linear set of equations that results from geometric constraints, giving the least squares location estimate. This technique is adopted by the GPS system [19], and it requires at least three ANs to estimate the location on a plane. Although computationally attractive, it is quite sensitive to errors on the relative distance estimates. A different natural localization strategy, based on maximum ratio combining of measurements [20], considers the position of the sensing static nodes as an estimate of the location of the moving agent. The location of the target is, thus, obtained by a convex weighted combination of the static node positions, where the weight that is associated with each static node is proportional to the RSS value or, equivalently, inversely proportional to the estimated distance. This approach is even simpler than triangulation but gives wrong answers if the target node is close to the border or outside of the WSN-covered area.

So far, the described localization procedures simply provide an estimate of the target position based on the measurements at some time instant t. However, better estimates can, in principle, be obtained by also using past measurements combined with a stochastic model of the MN dynamics, such as a random-walk model. Classical approaches for tracking are based on Kalman filters [21] or more general Bayesian filters like particle filters [7], [17], which act similarly to low-pass filters on the instantaneous position estimates. This dynamic-based tracking pairs particularly well with the stochastic RSS map-based localization since they are both probabilistic models, and they will be developed in detail in Section III.

III. System Modeling

This algorithm is based on the measured RSS over the links between ANs and an MN, which is sensed by the MN; a suitable *a priori map* containing the RSS distribution over the area of interest is built. The MN dynamics are modeled as a Markovian homogeneous first-order process and, therefore, allow Bayesian filtering to estimate and track the MN position. In this context, the WSNs act in a centralized fashion since the MN is supposed to be a smart sensor or to be connected to a processing unit (e.g., a PDA or a laptop). The problem presented here deals with a single MN, but the approach can easily be extended to the multiobject tracking.

A. RSS Map Stochastic Modeling

Before formalizing the localization and tracking problem, one observation is in order, regarding the 2-D reduction of the problem (neglecting the vertical direction), which is intrinsically 3-D. In this context, however, the indoor localization is considered where the 3-D environment is reduced to the collection of planar layers, which is a situation that is well suited for building floors, where there is limited crosstalk among sensors belonging to different floors. Note that if there is a need to also track the vertical position, the extension of the proposed design to the 3-D case can be carried out at the price of increasing the complexity of the algorithms and the necessity of introducing network variability w.r.t. the vertical coordinate, also within the same floor, to avoid degeneration of the estimation.

The formalization of the problem proceeds as follows. Let the region denoted as $\mathcal{X} \subset \mathbb{R}^2$ be the monitored area; a WSN that is composed of L ANs (also called beacons) is deployed over region $\mathcal{X}$ at fixed and known locations $\mathbf{s}^{(l)} = [s_1^{(l)}\ s_2^{(l)}]^T \in \mathcal{X}$, $l = 1, \ldots, L$. Conversely, an MN is free to move in $\mathcal{X}$, and its position $\mathbf{x}_t = [x_{1,t}\ x_{2,t}]^T$ in the discrete time domain $t \in \mathbb{Z}_+$ has to be estimated as the outcome of the localization procedure.

As a matter of fact, the state $\mathbf{x}_t$ is not a directly measurable quantity, and thus, it has to be computed from L measurements that are exchanged at each time step between the MN and the ANs, i.e., $\mathbf{y}_t = [y_{1,t}, \ldots, y_{L,t}]^T$, $\mathbf{y}_t \in \mathbb{R}^L$, where each measurement $y_{l,t}$ is the power (in decibels below 1 mW) of the signal that is transmitted by the lth AN as received by the MN when in the $\mathbf{x}_t$ location. Without getting into detail, a well-agreed model for the received power signal is a log-normal model of the channel model [22] that is also validated by ray-tracing techniques [14]; in terms of measurement variable $y_{l,t}$, this model yields the following:

$$y_{l,t} = \bar{y}_l(\mathbf{x}_t) + v_{l,t}, \qquad l = 1, \ldots, L \tag{1}$$

where $\bar{y}_l(\mathbf{x}_t)$ is a deterministic value accounting for the attenuation due to static obstacles and signal propagation, and $v_{l,t} \sim \mathcal{N}(0, \sigma_l^2(\mathbf{x}_t))$ indicates the random effects of people and small objects moving across the environment; both $\bar{y}_l(\mathbf{x}_t)$ and $\sigma_l(\mathbf{x}_t)$ are obtained via experimental campaigns.

According to (1) and taking into account the independence of L measurements, the probability of measuring $\mathbf{y}_t$ being the MN in $\mathbf{x}_t$ is a vector whose mean and variance, respectively, are

$$\bar{\mathbf{y}}_t = \begin{bmatrix} \bar{y}_1(\mathbf{x}_t) \\ \vdots \\ \bar{y}_L(\mathbf{x}_t) \end{bmatrix} \in \mathbb{R}^L$$

$$\mathbf{C}(\mathbf{x}_t) = \begin{bmatrix} \sigma_1^2(\mathbf{x}_t) & 0 & \cdots & \\ 0 & \sigma_2^2(\mathbf{x}_t) & & \\ \vdots & & \ddots & \\ & & & \sigma_L^2(\mathbf{x}_t) \end{bmatrix} \in \mathbb{R}^{L \times L}.$$

The probability density function (pdf) of each measurement $y_{l,t} \sim \mathcal{N}(\bar{y}_l(\mathbf{x}_t), \sigma_l^2(\mathbf{x}_t))$ is

$$p(y_{l,t}|\mathbf{x}_t) = \frac{1}{(2\pi)^{1/2}\sigma_l(\mathbf{x}_t)} e^{-\frac{\left(y_{l,t} - \bar{y}_l(\mathbf{x}_t)\right)^2}{2\sigma_l^2(\mathbf{x}_t)}} \tag{2}$$

yielding the global conditioned pdf for the whole set $\mathbf{y}_t$

$$p(\mathbf{y}_t|\mathbf{x}_t) = \frac{1}{(2\pi)^{L/2}\left|\mathbf{C}(\mathbf{x}_t)\right|^{1/2}} e^{-\frac{1}{2}(\mathbf{y}_t-\bar{\mathbf{y}}_t)^T\mathbf{C}^{-1}(\mathbf{x}_t)(\mathbf{y}_t-\bar{\mathbf{y}}_t)}. \tag{3}$$

In reality, however, the transmission channel is far from the ideal model (1) and presents weak signal events, which are ignored by the MN device, and proper packet loss phenomena. To take into account these issues, the packet-arrival process is modeled as a random variable γ_l that is assumed to be stationary and independent and identically distributed. More in detail, $\gamma_l(\mathbf{x}_t)$, which is related to the MN in $\mathbf{x}_t$ receiving from the lth AN, is a Bernoulli process with success probability $\lambda_l(\mathbf{x}_t)$, whose value is chosen according to experimental considerations; that is, $\gamma_l(\mathbf{x}_t)$ assumes a unitary value with probability $\lambda_l(\mathbf{x}_t)$ when the transmitted signal is received; otherwise, $\gamma_l(\mathbf{x}_t) = 0$, and a packet loss occurs. By doing so, the measurement vector $\mathbf{y}_t$ presents informative data entries $\tilde{y}_{l,t}$ only with probability $\lambda_l(\mathbf{x}_t)$, i.e.,

$$\tilde{y}_{l,t} = y_{l,t} \text{ if } \gamma_l(\mathbf{x}_t) = 1. \tag{4}$$

Otherwise, a default value y_0 is used to indicate the measurement corruption. From these considerations, the probability of receiving the measurement $\tilde{y}_{l,t}$ conditioned to state $\mathbf{x}_t$ takes into account the two contributions that are related to received and missed signals, thus modifying to

$$p(\tilde{y}_{l,t}|\mathbf{x}_t) = \lambda_l(\mathbf{x}_t)\frac{1}{\sqrt{2\pi\sigma_l^2(\mathbf{x}_t)}} e^{-\frac{\left(y_{l,t}-\bar{y}_l(\mathbf{x}_t)\right)^2}{2\sigma_l^2(\mathbf{x}_t)}} + \left(1-\lambda_l(\mathbf{x}_t)\right)\delta(y_{l,t}-y_0). \tag{5}$$

Since we suppose the L measurements to be mutually independent, the following formula holds for the whole observation $\mathbf{y}_t$:

$$p(\mathbf{y}_t|\mathbf{x}_t) = \prod_{l\in\mathcal{R}} \lambda_l(\mathbf{x}_t)\frac{1}{\sqrt{2\pi\sigma_l^2(\mathbf{x}_t)}} e^{-\frac{(y_{l,t}-\bar{y}_l(\mathbf{x}_t))^2}{2\sigma_l^2(\mathbf{x}_t)}} \cdot \prod_{m\in\mathcal{Q}} \left(1-\lambda_m(\mathbf{x}_t)\right)\delta(y_{l,t}-y_0) \tag{6}$$

where $\mathcal{R}$ represents the subset of received AN signals, and $\mathcal{Q}$ is the subset of missed ones at time t. The quantities $\bar{y}_l(\mathbf{x})$, $\sigma_l(\mathbf{x})$, and $\lambda_l(\mathbf{x})$ are known for every possible state position $\mathbf{x} \in \mathcal{X}$ and for every AN $l = 1, \ldots, L$; their values are being obtained through an offline gathering, as shown later in this paper.

The solution to the localization problem, that is, to find an estimate of position $\mathbf{x}_t$ given the $\mathbf{y}_t$ measurements, can be obtained in a Bayesian setting (7) by exploiting the whole measurement series $\{\mathbf{y}_1, \ldots, \mathbf{y}_t\}$ to obtain a nonlinear recursive filter, i.e.,

$$\widehat{\mathbf{x}}_t = \mathbb{E}[\mathbf{x}_t \mid \mathbf{y}_1, \ldots, \mathbf{y}_t] = \int_{\mathcal{X}} \mathbf{x}_t p(\mathbf{x}_t \mid \mathbf{y}_1, \ldots, \mathbf{y}_t) d\mathbf{x}_t. \tag{7}$$

This approach basically corresponds to the extension of the minimum-mean-square-error Kalman filter concept to a nonlinear context and in the presence of non-Gaussian driving processes (as, in general, for the application of interest).

The *a posteriori* pdf depends on a memory-less term and a memory-bearing one, which follows

$$p(\mathbf{x}_t \mid \mathbf{y}_1, \ldots, \mathbf{y}_t) \propto p(\mathbf{y}_t \mid \mathbf{x}_t) p(\mathbf{x}_t \mid \mathbf{y}_1, \ldots, \mathbf{y}_{t-1}) \tag{8}$$

where $p(\mathbf{y}_t|\mathbf{x}_t)$ is obtained through (6). On the other hand, since obtaining the *a priori* pdf by analytically solving the Chapman–Kolmogorov equation

$$p(\mathbf{x}_t \mid \mathbf{y}_1, \ldots, \mathbf{y}_{t-1}) = \int_{\mathcal{X}} p(\mathbf{x}_t \mid \mathbf{x}_{t-1}) \times p(\mathbf{x}_{t-1}|\mathbf{y}_1, \ldots, \mathbf{y}_{t-1}) d\mathbf{x}_{t-1},\ t > 1 \tag{9}$$

is not a viable solution, a particle filter [23] is used to produce an approximation of the *a priori* pdf as an equally weighted sum of S Dirac pulses that are irregularly centered on a set of particles $\{\mathbf{x}_t^{(s)}\}_{s=1}^S$, i.e.,

$$p(\mathbf{x}_t \mid \mathbf{y}_1, \ldots, \mathbf{y}_{t-1}) \approx \frac{1}{S}\sum_{s=1}^{S} \delta\left(\mathbf{x}_t - \mathbf{x}_t^{(s)}\right). \tag{10}$$

In this respect, from (6), (8), and (10), the following relation holds:

$$p(\mathbf{x}_t|\mathbf{y}_1, \ldots, \mathbf{y}_t) \approx \sum_{s=1}^{S} a_t^{(s)} \delta\left(\mathbf{x}_t - \mathbf{x}_t^{(s)}\right) \tag{11}$$

where $a_t^{(s)} \propto p(\mathbf{y}_t|\mathbf{x}_t^{(s)})$, $\sum_{s=1}^S a_t^{(s)} = 1$ (weight normalization), and the position estimate is finally given by

$$\widehat{\mathbf{x}}_t = \mathbb{E}[\mathbf{x}_t \mid \mathbf{y}_1, \ldots, \mathbf{y}_t] = \int_{\mathcal{X}} \mathbf{x}_t p(\mathbf{x}_t \mid \mathbf{y}_1, \ldots, \mathbf{y}_t) d\mathbf{x}_t \approx \sum_{s=1}^{S} a_t^{(s)} \mathbf{x}_t^{(s)} \tag{12}$$

where the $a_t^{(s)}$ terms take into account the channel and the packet-loss modeling.

As a further remark, adopting the packet-loss modeling allows the definition of weights that are more consistent with the effective behavior of the network and, thus, boiling down to a more balanced estimation procedure for the MN location, where measurements from robust channels are preferred.

A final note concerns the adopted particle filter, which is a sequential importance resampling particle filter [23]. At every discrete time t, the algorithm recursively computes a set of S particles and their weights $a_t^{(s)}, s = 1, \ldots, S$ and, therefore, approximating the *a posteriori* pdf $p(\mathbf{x}_t|\mathbf{y}_1, \ldots, \mathbf{y}_t)$. At the same time, to avoid degeneracy problems (a few particles with heavy weights), the resampling step is done at every iteration: In doing so, more equally weighted particles are placed instead of a "heavy" single particle so that every state probability does not change on the whole.

B. MN Dynamics

The MN dynamics are assumed to be a 2-D random walk, which is modeled by a first-order homogeneous Markov process, i.e.,

$$\mathbf{x}_t = \mathbf{x}_{t-1} + \mathbf{w}_t \tag{13}$$

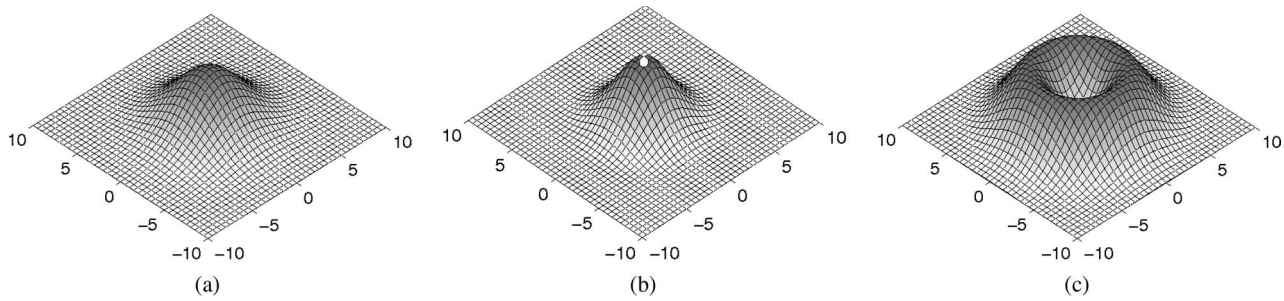

Fig. 1. Shape of the driving process for the MN dynamics. (a) Gaussian pdf. (b) Beta pdf. (c) Gaussian ring pdf.

where $\mathbf{w}_t$ denotes the driving process. The probabilistic model of the state evolution accords to $p(\mathbf{x}_t|\mathbf{x}_{t-1}) = f_{\mathbf{w}}(\mathbf{x}_t - \mathbf{x}_{t-1})$, where $f_{\mathbf{w}}$ is the $\mathbf{w}$ pdf. The initialization of the state, in terms of $p(\mathbf{x}_1), \forall \mathbf{x}_1 \in \mathcal{X}$, can be obtained from *a priori* information on the MN position or from higher level information that is related to the environment structure (e.g., presence of entrances or notable access points); otherwise, a uniform distribution is adopted.

The modeled process is driven by a noise term $\mathbf{w}_t$, whose features are determined by some hypotheses on the node dynamics. Preliminarily introducing polar coordinates $\rho = \|\mathbf{x}_t - \mathbf{x}_{t-1}\|$ and $\theta = \arctan(x_{2,t} - x_{2,t-1}/x_{1,t} - x_{1,t-1})$, the following three dynamic models are considered, also assuming average walking and running speed of about, respectively, 1.3 and 4.4 m/s (in this context, a sampling time of 1 s is set).

- *Gaussian pdf.* At each time step, the steady condition is the most probable behavior, whereas the probability of moving decreases with the traveled distance in any direction [16], [17]; the standard deviation σ_v is set to 3, which means that the majority (68%) of the MN movements are characterized by a velocity that is smaller than 3 m/s [see Fig. 1(a)]. In polar coordinates, this pdf can be expressed as

$$f_{\mathbf{w}}(\rho) = \frac{1}{2\pi^{1/2}\sigma_v} e^{-\frac{\rho^2}{2\sigma_v^2}}, \quad f_{\mathbf{w}}(\theta) = \frac{1}{2\pi}. \tag{14}$$

- *Beta pdf.* A refinement to the Gaussian distribution is obtained through a Beta function that ascribes nonnull probability values only when moving within a finite distance from the past position, thus discouraging the steady position while preventing, at the same time, unfeasible long-distance movements, i.e.,

$$f_{\mathbf{w}}(\rho) \propto \frac{1}{B(a,b)} \rho^{a-1}(1-\rho)^{b-1} \mathbb{I}_{[0,\rho_{\mathrm{MAX}}]}(\rho), f_{\mathbf{w}}(\theta) = \frac{1}{2\pi} \tag{15}$$

  where $B(a,b)$ is the Beta function $B(a,b) = \int_0^1 \tau^{a-1}(1-\tau)^{b-1} d\tau$, and $\mathbb{I}$ is the indicator function; in the considered model, the pdf shows high values between 0 and 2 m/s and rapidly decreases to zero between 3 and 5 m/s [see Fig. 1(b); $a = 1.28$, and $b = 3.6, \rho_{\mathrm{MAX}} = 5$].
- *Gaussian ring pdf.* A more realistic case appears to be that where the steady position is given a null probability, and the most probable traveling speed is modeled with a Gaussian pdf with mean value $\bar{\rho} = 1.5$ m and standard deviation $\sigma_v = 2$ m, resulting in a uniform ring distribution [see Fig. 1(c)].

Further walk models could anyway be adopted, such as, for example, a nonisotropic pdf that, in some sense, discourages any sudden change of direction.

C. Map Interpolation

Once the problem has been clearly stated and the theoretical framework has been described in detail, a further remark on a more practical ground is in order.

High-precision estimates require the definition of a fine grid of possible *a priori* particle positions $\mathbf{x}^{(m)}$, which is in contrast to the need for an easy offline data gathering. Hence, a wider and comprehensive mesh for the measurement data $\mathbf{y}$ is built from the interpolation of the experimental data (obtained at N locations $\{\mathbf{z}^{(n)}\}_{n=1}^N$) over a finer grid of $M > N$ points, with Δ being the interpolation step, i.e.,

$$\{\mathbf{z}^{(n)}\}_{n=1}^N \subsetneq \{\mathbf{x}^{(m)}\}_{m=1}^M = \{[h\Delta\ k\Delta]^T \\ h \in [0,\ldots,H], k \in [0,\ldots,K]\} \subseteq \mathcal{X} \tag{16}$$

(although it is not required for the finer grid to be necessarily regular), where the area of interest measures $H\Delta \times K\Delta$. For the sake of simplicity, the average RSS $\bar{y}_l$ will be considered. The data gathering provides a set of values $\{\bar{y}_l(\mathbf{z}^{(n)})\}_{n=1}^N$, that is, the measurements of the lth beacon at the $\mathbf{z}$ locations. This can also be interpreted as an irregular N-sampling of a 2-D stochastic stationary signal, i.e.,

$$\bar{y}_l(\mathbf{x}_t) \approx \bar{y}_l\left(\mathbf{x}^{(m)}\right) = \sum_{n=1}^N c_n\left(\mathbf{x}^{(m)}\right) \bar{\mathbf{y}}_l\left(\mathbf{z}^{(n)}\right) \\ = \mathbf{Y}_l^T \cdot \mathbf{c}\left(\mathbf{x}^{(m)}\right), l = 1,\ldots,L, m = 1,\ldots,M \tag{17}$$

where $\bar{\mathbf{y}}_l$ is the N-dimensional measurement vector from the lth AN, and $\mathbf{c}$ is a vector of N coefficients that are related to the specific $\mathbf{x}^{(m)}$ location. Reasonably, the stochastic signal has an isotropic correlation function $r(\|\mathbf{x}^{(i)} - \mathbf{x}^{(j)}\|) = r(d)$, after which, the coefficients $c_n(\mathbf{x}^{(m)})$ are calculated by applying the *orthogonality principle* that gives Wiener–Hopf simultaneous equations [24] and, therefore, obtaining

$$\mathbf{c}\left(\mathbf{x}^{(m)}\right) = \mathbf{R}^{-1}\mathbf{r}\left(\mathbf{x}^{(m)}\right) \tag{18}$$

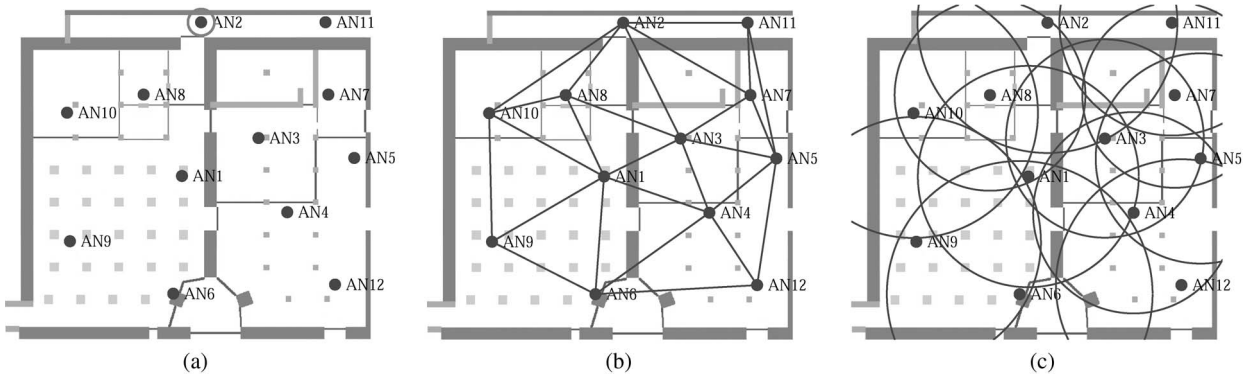

Fig. 2. Map of the simulation/experiment environment. (a) AN locations. The AN $\mathcal{V}_2$ is shown with a circle. (b) Delaunay triangulation. (c) Cell definition.

introducing $\mathbf{R}$ and $\mathbf{r}(\mathbf{x}^{(m)})$ for compactness of notation as

$$\mathbf{R} = \begin{bmatrix} r\left(\|\mathbf{z}^{(1)} - \mathbf{z}^{(1)}\|\right) & \cdots & r\left(\|\mathbf{z}^{(1)} - \mathbf{z}^{(N)}\|\right) \\ \vdots & & \vdots \\ r\left(\|\mathbf{z}^{(N)} - \mathbf{z}^{(1)}\|\right) & \cdots & r\left(\|\mathbf{z}^{(N)} - \mathbf{z}^{(N)}\|\right) \end{bmatrix}$$

$$\mathbf{r}\left(\mathbf{x}^{(m)}\right) = \begin{bmatrix} r\left(\|\mathbf{x}^{(m)} - \mathbf{z}^{(1)}\|\right) \\ \vdots \\ r\left(\|\mathbf{x}^{(m)} - \mathbf{z}^{(N)}\|\right) \end{bmatrix}.$$

Remarkably, when the interpolation location $\mathbf{x}^{(\bar{m})}$ coincides with the actual measurement position $\mathbf{z}^{(\bar{n})}$, the interpolation method provides the exact value $\bar{y}_l(\mathbf{x}^{(\bar{m})}) = \bar{y}_l(\mathbf{z}^{(\bar{n})})$. The same method is applied for σ_l^2 and for λ_l.

In this paper, the model given by (4)–(13) and here recalled

$$\begin{cases} \mathbf{x}_t = \mathbf{x}_{t-1} + \mathbf{w}_t \\ \tilde{y}_{l,t} = y_{l,t}, \qquad \text{if } \gamma_l(\mathbf{x}_t) = 1 \end{cases} \tag{19}$$

is studied and exploited in simulation (see Section IV) and implemented in real-world testbed experiments (see Section V).

IV. Simulations

Before entering the field of the code implementation for the experimental campaign, the algorithm is validated through MATLAB simulations based on the environment and the *a priori* maps that are obtained from the real experiments (see Section V for an accurate description).

First of all, the concept of *cell* is introduced. This idea is not so trivial since the AN locations are not defined according to a geometric displacement but obtained through a heuristic placement procedure (see Section V). After the set $\mathcal{V}$ of AN nodes is deployed [see Fig. 2(a)], a Delaunay triangulation procedure is performed to produce the edges $\mathcal{E}$ [see Fig. 2(b)]. From the so defined graph $\mathcal{G} = \{\mathcal{V}, \mathcal{E}\}$, the cell $\mathcal{C}_i$ that is associated with the ith beacon $\mathcal{V}_i$ is a circle that is centered on the $\mathcal{V}_i$ location, whose radius is the average length of the ith node out-edges. The circle radius is assumed to be the cell dimension [see Fig. 2(c)]. In the experimental and simulation setup, the complete area coverage is attained (12 ANs over 1500 m^2), with the mean cell dimension being $R = 12.12$ m with standard deviation $\sigma_R = 1.54$ m.

A second aspect concerning the generation of the *a priori* maps is related to the AN characterization in terms of signal power emission/receipt and packet-loss probability. In this respect, the environment is heavily affecting these phenomena, as can be seen, for example, in Fig. 3, which shows the interpolated maps of the RSS mean and variance, and the packet-transmission success probability corresponding to beacon $AN2$. The shape of these surfaces clearly highlights that the node is located at a T-junction between two long corridors.

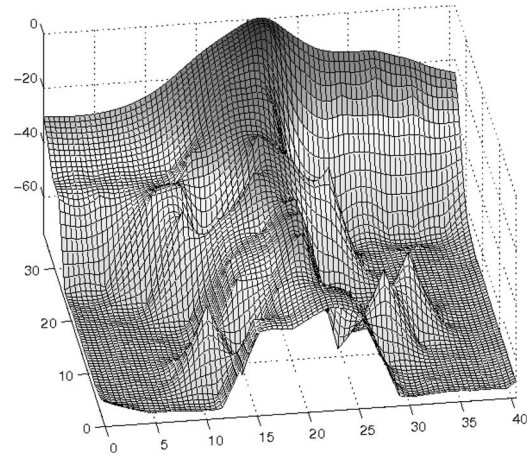

Fig. 3. Example of interpolated data from $AN2$ [highlighted in Fig. 2(a) with a circle]: Mean RSS (in decibels below 1 mW).

The track of an MN moving across the entire area avoiding walls and barriers is considered to test a long and widely distributed trajectory, and the experimental maps are employed. In these simulations, a Gaussian ring-driving process ($\bar{\rho} = 1.5$ m, $\sigma_v = 2$ m) is assumed in model (13).

A first issue concerns the inclusion of the packet-loss phenomena in the localization algorithm and its effects on the reconstruction performance w.r.t. similar approaches presented in the literature [7]. For readability's sake, in the following, the localization algorithm, including the packet loss, will be referred to as the with-packet-loss (WPL) algorithm, while neglecting it will be labeled as the no-packet-loss (NPL) algorithm. In simulation, it is shown that the performance of the WPL algorithm is 7%–15% better in terms of the mean localization error than that of the NPL procedure: In Fig. 4(a) and (b), an instance of the reconstructed path is shown in the two cases of the NPL and the WPL, also showing that the convergence of the WPL after a bad estimate is faster than that in the case of the NPL. Over a large number of simulations w.r.t. the simulation test path, the mean

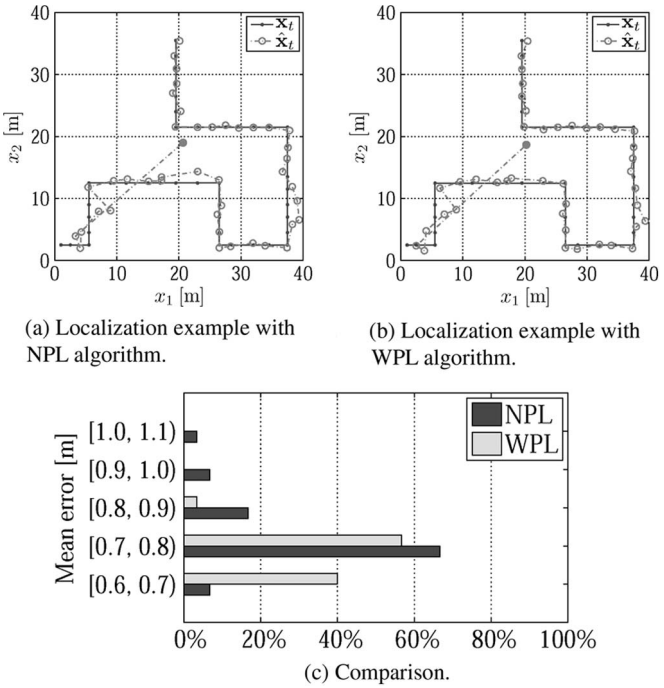

(a) Localization example with NPL algorithm.

(b) Localization example with WPL algorithm.

(c) Comparison.

Fig. 4. Packet loss versus nonpacket loss algorithm. An example of path reconstruction is given using the localization algorithm (a) without taking into account the packet loss probability (NPL) and (b) taking into account the packet loss (WPL). In both cases, a random initial condition is set (solid dot in the center of the area). (c) Comparison of the two performances is obtained by averaging the mean error over 30 simulations.

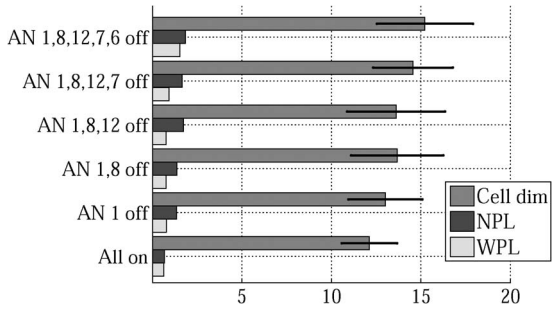

Fig. 5. Robustness analysis. The mean tracking error with dead motes obtained taking and without taking into account the packet loss is compared with cell dimension R; also, the cell dimension standard deviation σ_R is reported.

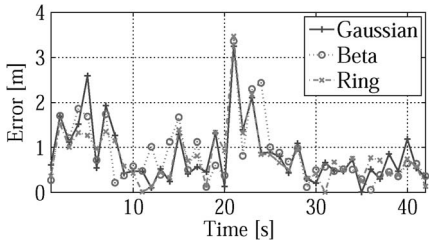

Fig. 6. Comparison among three driving processes for the MN dynamics.

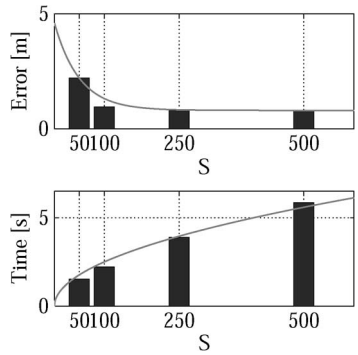

Fig. 7. Particle filter performances in the WPL algorithm. The number of particles versus mean error and computational time. The indicated time values refer to the completion of the whole simulation path.

error distribution proves the validity of the former approach [see Fig. 4(c)]: The error remains below the threshold of 0.7 m in around 40% of the trials (versus 7% obtained with the NPL), is below 0.8 m in 97% of the trials (versus 74% with the NPL), and is below 0.9 m in 100% of the trials (versus 90% with the NPL).

In addition, it is of fundamental interest to understand the whole network performance in relation to the robustness of the system to node failure, which is a major problem in WSNs. In this spirit, besides the lossy channel model, complete failure of nodes is artificially introduced in the AN network, gradually decreasing the cardinality of $\mathcal{V}$ (the number of beacons) from 12 to 7. The comparison between the performance of the two procedures NPL and WPL is summarized in Fig. 5: The mean tracking error is plotted against the cell dimension, which basically increases as the number of ANs decreases since the remaining set needs to grant coverage to a wider area. While the mean error that is obtained in the WPL case is lower than that in the NPL case, the ratio between the WPL mean error and the cell dimension also goes from about 6% up to 12%, which is, in any case, quite a satisfactory factor.

As a further issue, the MN dynamics is investigated w.r.t. the choice of the driving process in (13). Although of crucial theoretical interest for statistics analysis and modeling, for robustness' sake, this aspect should not play a key role in determining the performance of the tracking algorithm, and the simulations described in the following show that this feature is actually granted in the proposed framework. The trajectory reconstruction error shown in Fig. 6 highlights the substantial consistency of the estimated position w.r.t. the real data and confirms how the algorithm (in this case also accounting for the packet-loss phenomena using the WPL algorithm) is robust to these dynamic model uncertainty, keeping—in all cases—the error band, on average, below 1 m, which is much less than the cell dimension $R = 12.12$ m, with only a few localized peaks.

A final note regards the particle filter implementation and the chosen number of particles S. By varying S, it appears (see Fig. 7) that the estimation mean error is related to S through a decreasing exponential function, whereas the algorithm execution time approximately grows with the square root of S. The adopted number $S = 500$ grants good performance while keeping the global running time of the procedure well within both the simulation and real implementation timings.

V. Implementation and Experimental Results

Here, the implementation of the system in a real-world scenario and the preparation for the operational use are presented, which consist of two different tasks, namely, AN heuristic

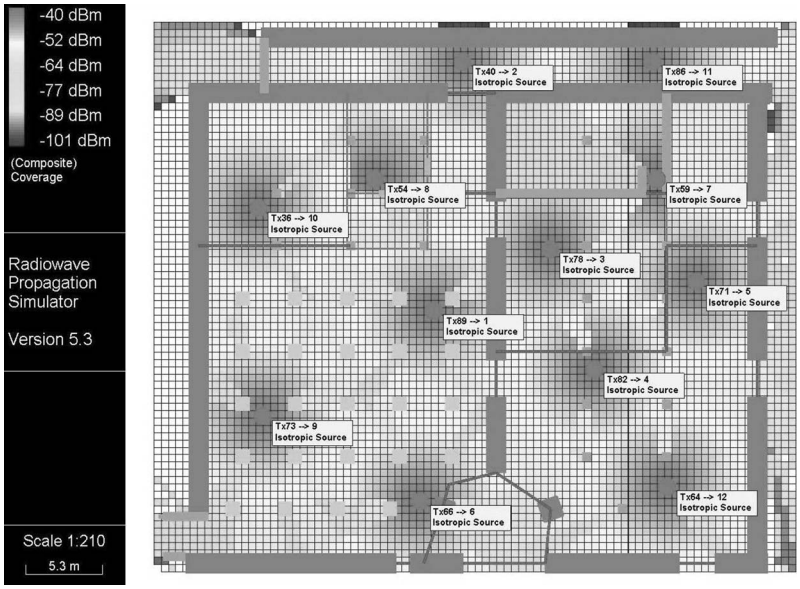

Fig. 8. RPS-simulated power distribution over the interested area. Thicker lines correspond to armored concrete walls and pillars, whereas thinner lines denote mesh fences that people can walk through using apposite doors.

deployment and data gathering for *a priori* maps. Also, some experimental results are discussed. The described infrastructure was realized in an industrial basement floor in use; the ambient measures 37 $\times$ 41 m, the area is about 1500 m^2 wide, and the ceiling is 3 m high, on average.

A. Beacon Deployment and Connectivity Analysis

The problem considered in the framework of this paper concerns large and sometimes critical environments, and indeed, the location of the testbed installation is characterized by reinforced concrete walls and pillars (over 1.5 m wide) and metallic fences by the presence of industrial uninterruptible power systems, electric boards, and high-voltage power cables. A WSN that is suitable for such an environment should have the following characteristics: low density, low consumption, low maintenance, and ease of installation. At the same time, to ensure a robust WSN design, the localization algorithm should not depend on the choice of the AN positions, and a little redundancy is needed w.r.t. the area coverage: A good tradeoff is given by imposing that the MN senses at least four ANs (almost) everywhere.[1]

Finding an optimal deployment of the ANs is, in general, a very difficult problem to solve [25]; in this context, a different suboptimal approach is preferred based on an accurate modeling of the ambient and on ray-tracing techniques [15]. A preliminary experimental connectivity analysis to support the actual node deployment is necessary. On-field tests show that the line-of-sight (LOS) link is 30 m long, whereas nonline-of-sight links are, on average, 20 m long. By rule of thumb, every beacon is assumed to cover a cell dimension of approximately 10–12 m, and 12 sensors are enough to guarantee robustness and stability to the WSN.

A software package (RPS Ver. 5.3) is used, which computes the power of an electromagnetic signal in a certain area considering signal attenuation in free space, reflection, diffraction, and scattering phenomena.[2] Every AN is modeled as an isotropic source with a carrying frequency of 2.4 GHz and a transmission power of 0 dBm (1.0 mW). A trial-and-error iteration procedure yields the final deployment to obtain a composite coverage of the area that is qualitatively balanced and quantitatively providing a signal intensity that is always higher than -65 dBm (see Fig. 8). Note that five ANs are positioned in each large subarea, and two ANs are placed along the corridor.

Remark: A further optimization can reduce to four the number of beacons in the two large subareas without preventing the localization method from working properly. Nonetheless, since the whole system is conceived to also run in emergency contexts, with one or more ANs damaged, some redundancy is kept w.r.t. the WSN coverage. Anyway, the small number of ANs grants easy and cheap installation of the WSN.

Remark: The RPS simulation assumes that all ANs are positioned at a 2-m height, and the receiver nodes are at a 1-m height. Even if these settings do not correspond to real work conditions [26], it is reasonable to suppose that the composite coverage of the area is actually close to the real one. Also, the localization and tracking algorithm is not influenced by a different height of ANs since all the computations refer to *a priori* maps that are gathered after the AN deployment. This fact allows the simplification to a 2-D problem.

B. A Priori Data Gathering

As explained in Section III, the algorithm requires *a priori* maps for the expected received power signal $\bar{y}_l(\mathbf{x})$, the random

[1]In some areas like closed rooms and narrow passages, only two ANs can be sensed. The correctness of the estimation is guaranteed by the stochastic modeling of the MN dynamics.

[2]The communication protocol that is used by the sensor motes imposes a carrying frequency belonging to [2400, 2483.5] MHz corresponding to a wavelength between 12.08 and 12.5 cm. Since the objects in the environment are larger than the wavelength, reflection, diffraction, and scattering take place.

effect due to small objects and people moving $\sigma_l^2(\mathbf{x})$, and the packet arrival probability $\lambda_l(\mathbf{x})$. A coarse almost regular grid is exploited, locating $N = 115$ gathering locations ($\{\mathbf{z}^{(n)}\}_{n=1}^{N} \subsetneq \mathcal{X}$); the MN is placed in each $\mathbf{z}^{(n)}$ position, listening to broadcasting ANs for $N_{TS} = 100$ time slots. During every interval, the MN stores the ID of the sensed ANs and the corresponding RSS; the length of each time slot (1000 ms_b, which is equal to[3] 976.56 ms) has been computed so that no data loss can occur, i.e., the MN is able to record up to 12 AN IDs and RSSs. The gathering campaign, nevertheless, reveals that no more than ten ANs can be sensed in some positions.

The radio chip provides an RSS indicator (RSSI), which is described by

$$\text{RSSI} = \text{RSS} + \text{RSS}_{\text{off}} \tag{20}$$

where RSS_{off} is an offset term varying from mote to mote. In general, the presence of this addendum makes a calibration necessary; in the specific case, no calibration is required if the same MN is used for offline data gathering and tracking. Therefore, in the following, we exploit the same notation by confusing RSSI with RSS.

Let $\mathcal{R}_l(\mathbf{z}^{(n)})$ be the subset of time slots when the lth AN is sensed by the MN placed in $\mathbf{z}^{(n)}$ once the maximum and minimum RSS values have been removed[4]; this solution will prove beneficial in the interpolation phase (see Section V-C). The expected value $\bar{y}_l(\mathbf{z}^{(n)})$ is given by

$$\bar{y}_l\left(\mathbf{z}^{(n)}\right) = \frac{1}{\left|\mathcal{R}_l\left(\mathbf{z}^{(n)}\right)\right|}\left(\sum_{i\in\mathcal{R}_l\left(\mathbf{z}^{(n)}\right)} y_l^{(i)}\left(\mathbf{z}^{(n)}\right)\right). \tag{21}$$

The expected received power signal for each gathering location $\bar{y}_l(\mathbf{z}^{(n)})$ is computed using a truncated propagation model, which means that when a node signal is not received at all, $\bar{y}_l(\mathbf{z}^{(n)}) = -70$ dBm, with the sensitivity of the node chip being -60 dBm. Similarly, the variance $\sigma_l^2(\mathbf{z}^{(n)})$ is computed as

$$\sigma_l^2\left(\mathbf{z}^{(n)}\right) = \frac{1}{\left|\mathcal{R}_l\left(\mathbf{z}^{(n)}\right)\right|}\left[\sum_{i\in\mathcal{R}_l\left(\mathbf{z}^{(n)}\right)}\left(y_l^{(i)}\left(\mathbf{z}^{(n)}\right) - \bar{y}_l\left(\mathbf{z}^{(n)}\right)\right)^2\right] \tag{22}$$

and, if $|\mathcal{R}_l(\mathbf{z}^{(n)})| \leq 1$, $\sigma_l^2(\mathbf{z}^{(n)}) = 25$ dBm^2 is chosen such that, if the received signal power is modeled as $\mathcal{N}(\bar{y}_l, \sigma_l^2)$, the probability of receiving a signal packet from the lth AN ($y_l \geq -60$ dBm) is around 4%.

The transmission success probability $\lambda_l(\mathbf{z}^{(n)})$ results from

$$\lambda_l\left(\mathbf{z}^{(n)}\right) = \max\left[\lambda_{\min}, \min\left(\frac{\left|\mathcal{R}_l\left(\mathbf{z}^{(n)}\right)\right|}{N_{TS}}, \lambda_{\text{MAX}}\right)\right] \tag{23}$$

which limits the range value $\lambda_l(\mathbf{z}^{(n)}) \in [\lambda_{\min}, \lambda_{MAX}] = [0.03, 0.97]$; this practical constraint is motivated by the limited time that is employed for the offline gathering together with the high average LOS link w.r.t. the dimension of the environment.

C. Map Interpolation

In the actual setup, the fine position estimate grid $\{\mathbf{x}^{(m)}\}_{m=1}^{M} \subseteq \mathcal{X}$ is a regular 2-D grid with $\Delta = 0.5$ m. An isotropic correlation function is assumed for the interpolation procedure, as proposed in [24] for the estimation of 2-D continuous fields, i.e.,

$$r(d) = e^{-\frac{d}{d_0}} \tag{24}$$

where d_0 refers to the weight attributed to distant data: Higher values for d_0 yield to smoother map surfaces, while lower values provide beveled ones. Empirical considerations suggest $d_0 = 20$ for both the expected power $\bar{y}_l$ and the variance σ_l^2, and $d_0 = 10$ for the probability λ_l. To avoid boundary effects, some fictitious gathering positions along the contour are added, whose values $\bar{y}_l$, σ_l^2, and λ_l are equal to those of the nearest surveying locations. Additional attention must be paid to variance and probability interpolation: By structure, these parameters are bounded to $\sigma_l^2(\mathbf{x}) \geq \sigma_{\min}^2$ and $\lambda_{\min} \leq \lambda_l(\mathbf{x}) \leq \lambda_{\text{MAX}}, \forall \mathbf{x}$, where $\sigma_{\min}^2 = 0.01$ dBm^2 is the minimum observed variance value.

D. Hardware and Software Details

The ANs and the MN employed in this paper are Tmote Sky [27], low-consumption motes provided with a Texas Instruments MSP430 microcontroller (8 MHz, 10-kB random access memory, 48-kB Flash memory), and a radio chip Chipcon CC420 [28], which implements the communication protocol IEEE 802.15.4 [29]. The MSP430 can turn the radio chip on and off and can modulate the transmission power, which, in this implementation, is kept constant at the maximum level. The motes are powered either by two AA batteries or via Universal Serial Bus (USB) connection. The former solution is chosen for the ANs (regularly checking batteries), and the latter is adopted for the MN, committing to a laptop PC the burden of algorithmic computation. To complete the description, motes employ an operating system for embedded device, i.e., TinyOS v. 1.1.15, which is programmed in nesC language [30].

In addition to the localization of the MN, the communication of its position outside the network is also considered, mimicking the presence of a remote coordination center. To this aim, a multihop transmission protocol is applied, routing the position estimate to a chosen AN that takes charge of the external connection. A policy is enforced that checks the novelty of a message before forwarding it to avoid data loop. Since the multihop protocol requires that every AN can sense and be sensed by at least another AN, to ensure robustness of the communication procedure, in the design phase, further constraint on the graph $\mathcal{G}$ is posed to be connected and

[3]The used hardware timer is in *binary milliseconds* (ms_b), that is, 1024 ticks every second.

[4]The cardinality of this set is denoted by $|\mathcal{R}_l(\mathbf{z}^{(n)})|$.

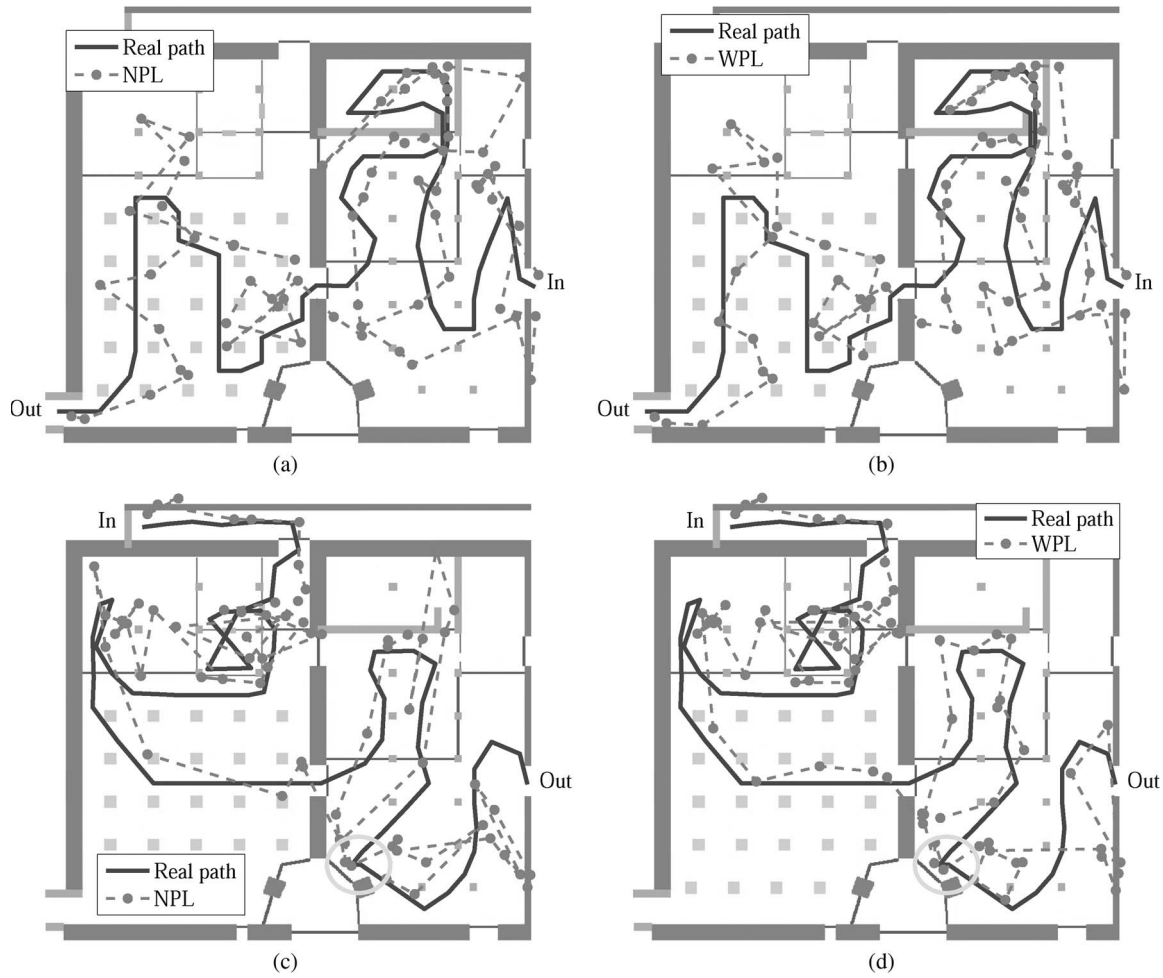

Fig. 9. Examples of position estimates of the operator track. (Solid line) Reference path. (Dots) Discrete position estimates. The stop of the operator (lower right side in path 2) is highlighted with a circle. (a) Path 1. NPL algorithm. (b) Path 1. WPL algorithm. (c) Path 2. NPL algorithm. (d) Path 2. WPL algorithm.

redundant.[5] The data packets from each AN are organized as follows:

- beacon ID (1 B);
- beacon position in the reference frame (2 B);
- transmission power (1 B).[6]

Indeed, a crucial point to grant good overall performance to the algorithm is represented by a correct choice of timings. The AN broadcast interval is set to 500 ms_b (488.28 ms), which is a good tradeoff to achieve low energy consumption while saving time. On the other hand, the MN sample time should be short enough to justify the approximation of the tracked position with a point, and concurrently, all operations of data receipt and position estimation through the particle filter must be accomplished. A good choice for the sample time length is $T = 2000$ ms_b (1953.12 ms): Within T, a listening time of 1000 ms_b assures that all packets are correctly received [29], and a further interval of 1000 ms_b is devoted to the algorithmic procedure; this involves the estimation of the MN position with the particle filter, which requires at most 300 ms_b, even with a large number of particles ($S = 500$), and leaves enough space (700 ms_b) for other ancillary tasks [31]. In the case that the estimated position is retransmitted to an external coordination center, doubling T is required in the specific implementation due to data transmission through USB requiring about 2000 ms_b.

E. Experimental Results

For the experiments, a human operator moving across the entire area is considered, following the routes shown in Fig. 9. In these experiments, the realistic measurement model (4) is employed, which includes packet loss phenomena. The initial position information $p(\mathbf{x}_1)$ [see (13)] is set to nonnull values only in correspondence to the actual entrances to the area, and the walk model is heuristically chosen as characterized by a Gaussian ring-driving process with $\bar{\rho} = 1.5$ m and $\sigma_v = 3$ m, if $T = 2000$ ms_b. These parameters are modified in the case of adopting different values of sampling time T, which is set according to the real-time requirements. The error estimate in the track reconstruction has a mean value in the range of 2.5–4.0 m, depending on the adopted sampling time, which

[5]These policies are often kept into account within the transmission protocols; however, it is also of interest to grant communication robustness from the network topology design.

[6]In this *a priori* map approach, the AN position, as well as the transmission power, is not used; nevertheless, three additional bytes affect the total communication time by 192 μs (the CC420 transmits data at 250 kb/s), which is negligible w.r.t. the length of the whole process (see Section V-D).

TABLE I
SIMULATION AND EXPERIMENT RESULTS. PERFORMANCES IN THE TWO CASES ARE COMPARED IN TERMS OF NODE DENSITY (AREA/NUMBER OF NODES), CELL AVERAGE RADIUS, AND MEAN LOCALIZATION ERROR

Nodes	Node Density	Mean Radius	Mean Error	Data Type
12	125 m^2/node	12.12 m	0.77 m	Sim.
11	136 m^2/node	13.01 m	0.90 m	Sim.
10	150 m^2/node	13.67 m	1.00 m	Sim.
9	166 m^2/node	13.61 m	1.13 m	Sim.
8	187 m^2/node	14.56 m	1.34 m	Sim.
7	214 m^2/node	15.22 m	1.79 m	Sim.
12	125 m^2/node	12.12 m	2.85 m	Exp. path 1
12	125 m^2/node	12.12 m	2.84 m	Exp. path 2

varies between $T = 2000$ ms_b and $T = 4000$ ms_b; in the latter case, since the distance in time between consecutive position increases (as well as its estimation uncertainty), higher error values are those expected and verified in the experiments. The comparison between the performance of the NPL and the WPL algorithms is also shown, in the case of real experiments, to account for the packet-loss phenomena that allows the amelioration of the position estimate quantitatively (in terms of the mean error), as already shown in Section IV. As the MN stops, estimations tend to accumulate around the correct location value, and the error diminishes [see Fig. 9(d)]. In any case, all error values remain quite small w.r.t. the dimensions of the cells and those characteristics of the environment, and better performance could also be reached with a dedicated C-language implementation.

VI. DISCUSSION

The results obtained both in simulation and real experiments are summarized in Table I, where the mean error value (averaged over several instances) is compared with the mean cell dimension. Only the WPL results are presented since the WPL algorithm consistently shows better performance w.r.t. the NPL algorithm in simulation and real experiments, lowering the mean error of about 7%–15% in both cases. Both the simulations and the experiments refer to the realistic lossy channel model, and the simulations are also conducted in the presence of complete failure of beacons. In the simulation case, the trajectory is that proposed in Section IV with the MN model that is characterized by a Gaussian ring-driving process. The experiments refer to a free trajectory of a human operator in the studied environment, again resorting to a Gaussian ring-driving process. A comment is now in order on the difference between the results obtained in the simulation and those obtained with real experiments. The AN map definition and data are the same for both series of experiments; also, the adopted model is similar, with the only difference given by the MN driving processes, which, in the case of the real experiments, is assumed to be characterized by more uncertainty (higher variance values) than that in the model used in the simulation. The source of the difference between the two performances is to be sought mainly in the actual MN behavior: In the simulation, measurements are provided by a realization of the ideal output equation (1), whereas in the real experiments, they are obtained from real measurements, which are, of course, not forced to follow a specific model.

VII. CONCLUSION

In this paper, the problem of localization and tracking in WSNs has been approached. In particular, this paper has focused on the design of a cheap and easy-to-deploy architecture for critical infrastructures, which, nevertheless, requires some effort for a preliminary setup campaign. The proposed tracking system architecture considers a static beacon network and an MN moving in it. In this spirit, an RSS map model of the monitored environment is built from experimental measurements, a stochastic model of the MN to be localized is employed, and the presence of lossy communication channel is taken into account. The formalization of the problem and the mathematical modeling have been developed and discussed in detail within the estimation theory framework. This approach is first validated in simulations, which also aims at providing a deeper insight into the dynamics of the MN and the placement of the ANs. One major contribution of this paper consists of the actual implementation of the system in an operative scenario, namely, the basement floor of an industrial building, where the localization experiments have been run. Within the condition variability of simulations and real experiments, the overall good performance of the system has been assessed in terms of reconstruction accuracy and robustness to node failure.

As a final note, both issues of network scalability and multi-object tracking can be dealt within this framework, while a more delicate aspect is that concerning the presence of a dynamic environment due to the exploitation of *a priori* maps.

ACKNOWLEDGMENT

The authors would like to thank L. Schenato for the extended and valuable discussions that have influenced this project and A. Zanella for discussions and suggestions during the final stages of this paper.

REFERENCES

[1] M. Kintner-Meyer and R. Conant, "Opportunities of wireless sensors and controls for building operation," *Energy Eng. J.*, vol. 102, no. 5, pp. 27–48, 2005.
[2] M. Nekovee, "Ad hoc sensor networks on the road: The promises and challenges of vehicular ad hoc networks," in *Proc. Workshop Ubiquitous Comput. e-Res.*, Edinburgh, U.K., May 2005.
[3] S. Oh, L. Schenato, and S. Sastry, "A hierarchical multiple-target tracking algorithm for sensor networks," in *Proc. IEEE Int. Conf. Robot. Autom.*, Barcelona, Spain, Apr. 2005, pp. 2197–2202.
[4] R. Szewczyk, E. Osterweil, J. Polastre, M. Hamilton, A. M. Mainwaring, and D. Estrin, "Habitat monitoring with sensor networks," *Commun. ACM*, vol. 47, no. 6, pp. 34–40, Jun. 2004.
[5] G. Tolle, J. Polastre, R. Szewczyk, N. Turner, K. Tu, P. Buonadonna, S. Burgess, D. Gay, W. Hong, T. Dawson, and D. Culler, "A macroscope in the redwoods," in *Proc. ACM SenSys*, San Diego, CA, Nov. 2005, pp. 51–63.
[6] A. Willig and K. Matheus, "Wireless technology in industrial networks," *Proc. IEEE*, vol. 93, no. 6, pp. 1130–1151, Jun. 2005.
[7] C. Morelli, V. Rampa, M. Nicoli, U. Spagnolini, and C. Alippi, "Particle filters for RSS-based localization in wireless sensor networks: An experimental study," in *Proc. IEEE Int. Conf. Acoust., Speech Signal Process.*, 2006, pp. 957–960.
[8] C. Swedberg, Chicago Fire Dept. Tests ZigBee-Based RFID System, Oct. 2006, [Online]. Available: http://www.rfidjournal.com/article/articleview/2717/1/1/#cmt3769
[9] R. Peng and M. L. Sichitiu, "Angle of arrival localization for wireless sensor networks," in *Proc. IEEE Conf. Sensor Ad Hoc Commun. Netw.*, Reston, VA, Sep. 2006, pp. 374–382.

[10] A. Smith, H. Balakrishnan, M. Goraczko, and N. B. Priyantha, "Tracking moving devices with the cricket location system," in *Proc. Int. Conf. Mobisys*, Boston, MA, Jun. 2004, pp. 190–202.
[11] Y.-T. Chan, W.-Y. Tsui, H.-C. So, and P.-C. Ching, "Time-of-arrival based localization under NLOS conditions," *IEEE Trans. Veh. Technol.*, vol. 55, no. 1, pp. 17–24, Jan. 2006.
[12] P. Bahl and V. N. Padmanabhan, "RADAR: An in-building RF-based user location and tracking system," in *Proc. IEEE INFOCOMM*, Jan. 2000, pp. 775–784.
[13] K. Lorincz and M. Welsh, "MoteTrack: A robust, decentralized approach to RF-based location tracking," *Pers. Ubiquitous Comput.*, vol. 11, no. 6, pp. 489–503, Aug. 2006.
[14] U. Spagnolini and A. Bosisio, "Indoor localization by attenuation maps: Model-based interpolation for random medium," in *Proc. ICEAA*, Sep. 2005, pp. 1–4.
[15] R. A. Valenzuela, "Ray tracing prediction of indoor radio propagation," in *Proc. IEEE Int. Symp. Pers., Indoor Mobile Radio Commun.*, 1994, vol. 1, pp. 140–144.
[16] C. Morelli, M. Nicoli, V. Rampa, and U. Spagnolini, "Hidden Markov models for radio localization in mixed LOS/NLOS conditions," *IEEE Trans. Signal Process.*, vol. 55, no. 4, pp. 1525–1542, Apr. 2007.
[17] H. Ren and M. Q. H. Meng, "Power adaptive localization algorithm for wireless sensor networks using particle filter," *IEEE Trans. Veh. Technol.*, vol. 58, no. 5, pp. 2498–2508, Jun. 2009.
[18] N. Patwari, "Location estimation in sensor networks," Ph.D. dissertation, Univ. Michigan, Ann Arbor, MI, 2005.
[19] Z. Li, W. Trappe, Y. Zhang, and B. Nath, "Robust statistical methods for securing wireless localization in sensor networks," in *Proc. IPSN*, 2005, pp. 91–98.
[20] L. Song and D. Hatzinakos, "A cross-layer architecture of wireless sensor networks for target tracking," *IEEE/ACM Trans. Netw.*, vol. 15, no. 1, pp. 145–158, Feb. 2007.
[21] Y. Bar-Shalom, X. R. Li, and T. Kirubarajan, *Estimation With Applications to Tracking and Navigation: Theory, Algorithms and Software*. Hoboken, NJ: Wiley, 2001.
[22] A. Goldsmith, *Wireless Communications*. New York: Cambridge Univ. Press, 2005.
[23] M. S. Arulampalam, S. Maskell, N. Gornod, and T. Clapp, "A tutorial on particle filters for on-line non-linear/non-Gaussian Bayesian tracking," *IEEE Trans. Signal Process.*, vol. 50, no. 2, pp. 174–188, Feb. 2002.
[24] G. Bolondi, F. Rocco, and S. Zanoletti, "Automatic contouring of faulted subsurfaces," *Geophys.*, vol. 41, no. 6, pp. 1377–1393, Dec. 1976.
[25] N. Bulusu, J. Heidemann, and D. Estrin, "Density adaptive algorithms for beacon placement in wireless sensor networks," Univ. Calif., Los Angeles, Los Angeles, CA, Tech. Rep. UCLA-CS-010013, 2001.
[26] L. E. Foong, C. Wang, and L. Xiao, "A study of radio signal behaviors in complex environments," Comput. Sci. Dept., Michigan State Univ., East Lansing, MI, 2006.
[27] *Tmote Sky: Datasheet*, Moteiv Corporation, San Francisco, CA, Nov. 2006. [Online]. Available: http://www.eecs.harvard.edu/~konrad/projects/shimmer/references/tmote-sky-datasheet.pdf
[28] *SmartRF CC2420 Datasheet (revision 1.3)*, Chipcon AS, Oslo, Norway, Oct. 2005. [Online]. Available: ttp://www-inst.eecs.berkeley.edu/cs150/~Documents/CC2420.pdf
[29] *802.15.4: Part 15.4: Wireless Medium Access Control (MAC) and Physical Layer (PHY) Specifications for Low-Rate Wireless Personal Area Networks (LR-WPANs)*, IEEE P802.15, 2003.
[30] D. Gay, P. Lewis, R. von Behren, M. Welsh, E. Brewer, and D. Culler, "The nesC language: A holistic approach to network embedded systems," in *Proc. ACM SIGPLAN Conf. Program. Language Des. Implementation*, Jun. 2003, pp. 1–11.
[31] *PPP in HDLC-Like Framing*, IETF, Jul. 1994. [Online]. Available: http://www.ietf.org/rfc/rfc1662.txt

Angelo Cenedese received the Laurea degree in 1999 and the Ph.D. degree in 2004, both from the University of Padova, Padova, Italy.

He is currently an Assistant Professor with the Department of Engineering and Management, University of Padova, Vicenza, Italy. He has held several visiting positions with international institutions: the Japan Atomic Energy Research Institute, Naka, Japan, in 2000; the United Kingdom Atomic Energy Authority–Joint European Torus Laboratory, Oxford, U.K., in 2001–2004; General Atomics, San Diego, CA, in 2004; and the University of California, Los Angeles, in 2010. He has been involved in European Union projects on control and diagnostics of nuclear fusion devices, on methodologies for adaptive optics systems, and on estimation and control in distributed networked systems. He is a coauthor of more than 40 papers. He has three international patent applications on the field of surveillance sensor networks under submission. His research interests include the fields of modeling, control theory and its applications, active vision, sensor and actuator networks, with particular attention to environmental monitoring and control, and surveillance networks.

Giulia Ortolan received the M.S. degree in automation from the University of Padova, Padova, Italy, where she is currently working toward the Ph.D. degree in information engineering.

In 2010, she was a Visiting Scholar with the Department of Mathematics, University of California, San Diego. Her research interests include geometric mechanics, variational integrators for rigid body dynamics, and geometric integration on homogeneous spaces.

Marco Bertinato received the M.S. degree in automation from the University of Padova, Padova, Italy.

He was with the Department of Information Engineering, University of Padova, where he developed heating, ventilating, and air conditioning genetic control systems. He is currently a Consultant with the Aprilia Racing S.r.l., Piaggio & Co. Group, R&D Department, working on motorbike dynamics and engine control for racing applications (SBK, SST, MX1, S1 World Championship, and NPO Rally).